MRS Advances
https://doi.org/10.1557/s43580-023-00514-4

ORIGINAL PAPER

Nonequilibrium carrier dynamics in $FeSe_{0.8}Te_{0.2}$

Alexander Bartenev[1] · Roman Kolodka[1] · Camilo Verbel[1] · Manuel Lozano[1] · Felix Fernandez[1] · Armando Rua[1] · Sergiy Lysenko[1]

Received: 18 November 2022 / Accepted: 24 January 2023

Abstract
We report on the nonequilibrium dynamics of photoinduced collective excitations in $FeSe_{0.8}Te_{0.2}$ superconducting (SC) thin film. The obtained transient reflectance traces show three distinct regions attributed to different dynamical processes. First two processes are observed within a sub-picosecond scale and are associated with photoexcitation of quasi-particles (QP). The first process is attributed to QPs accumulation and is sensitive to structural anisotropy. We use nematicity measurements to determine its time constant. The electron–phonon coupling constant of $\lambda = 0.2$ was derived and is consistent with previous studies for similar materials. Strong acoustic phonons generation was observed on a longer timescale.

Introduction

Recent studies of hidden nematicity and spin subsystem in FeSe by the polarized femtosecond pump–probe spectroscopy [1] show two distinct relaxation components in transient reflectivity signal. A correlation was found between the topology of the Fermi surface and the magnetism. Simultaneous probing of the electronic structure and the magnetic interactions through quasiparticle dynamics reveals both the electronic and magnetic nematicity in FeSe below and far above the structural phase transition ($T_S = 90$ K), up to ~ 200 K. Transient reflectivity measurements reveal unique information about QP relaxation processes [2, 3] such as electron–electron and electron–phonon scattering, optical [4] and acoustic phonons generation. Experimental results are greatly expanded by theoretical advances and are widely used to relate QP relaxation time to the second moment of the Eliashberg function $\lambda < \omega^2 >$, from which electron–phonon coupling (EPC) constant λ can be derived [2, 4] if main contributing phonon modes are known [3]. Due to relatively simple crystal structure and intriguing electrical and physical characteristics, FeSe superconductors and related systems have received much attention. In the Fe(Se,Te) system, Se can be replaced with Te to increase T_c up to 24 K [5–8], and superconductivity can sustain throughout a wide composition range. Unlike other iron pnictides, as $BaFe_2As_2$ [3, 9] or FeSe [2], there are fewer results on nonequilibrium carrier dynamics reported for $FeSe_xTe_{1-x}$, especially in higher pump fluences range (above 1 mJ/cm^2). Ultrafast optical spectroscopy is a powerful tool for investigating the ultrafast dynamics of excited states in quantum materials and is very attractive to probe QP dynamics in Fe(Se,Te) systems. It provides unique information about interactions between QPs and different degrees of freedom in superconductors [2, 10–12].

In this work, we report on the photoexcited dynamics of $FeSe_{0.8}Te_{0.2}$ within picosecond time domain. The measurements were performed at a relatively high fluence excitation regime. The nematicity measurements are used both for the identification of the nematicity transition temperature and the time-constant evaluation of the processes straight after the light excitation. We examine EPC strength by obtaining the second moment of the Eliashberg function. The acoustic phonons generation and decay are observed. Here we provide a phenomenological model, identify phonon modes, and their lifetimes.

Materials and methods

Epitaxial $FeSe_{0.8}Te_{0.2}$ films of 290 nm thickness were grown on CaF_2 single-crystal substrates by pulsed laser deposition (PLD). The ablation of the premixed FeSeTe target was performed at 10^{-6} Torr chamber pressure by excimer laser (Lambda Physik Compex 110) with 1.5 J/cm^2 fluence.

✉ Roman Kolodka
roman.kolodka@upr.edu

[1] Department of Physics, University of Puerto Rico, Mayaguez, PR 00681, USA

Published online: 13 February 2023

During the deposition process, the substrate temperature was fixed at 573 K. The SC properties were tuned by varying the strain level by altering the film thickness of the epitaxial film. The thinner the film was, the better SC properties it showed, down to the critical thickness, when superconductivity vanished.

In pump-probe measurements, we used the Spectra-Physics Ti:Sapphire femtosecond laser system with the central wavelength of 800 nm and a pulse duration of 35 fs. The pulse duration is the factor that limits the temporal resolution of our setup. The pump-probe experiments were carried out in reflection geometry, with the adjustable pump fluence of up to 8 mJ/cm^2. The pump and probe pulses, of the same wavelength, were overlapped on the sample surface, and probe intensity was substantially reduced by a neutral density filter to avoid its nonlinear interaction with the sample. For the precise control of pump power, the pump beam passes through the computer-controlled $\lambda/2$ waveplate combined with the Glan polarizer. For nematicity measurements, probe polarization was set to circular and detected in two orthogonal polarizations through the Wollaston prism. SRS Boxcar was used to process the signal from the photodetector. A closed-cycle cryostat with a minimum guaranteed temperature of 7.5 K was applied with 0.1 K temperature control precision.

Results and discussion

Electron phonon relaxation dynamics

After photoexcitation, the $FeSe_{0.8}Te_{0.2}$ material experiences a subsequent multi-step thermalization process. Figure 1a shows traces of the relative change in reflectivity at the 8 K sample temperature. The exponential fit shows a good approximation of the experimental data. It can be seen that the scanning traces after t > 0 ps are composed of both increasing and decreasing components, whose amplitude and lifetime vary both with fluence and temperature. A change in the transient signal $|\Delta R/R(t)|$ is proportional to the density of photoexcited free carriers [11, 13], as the absorption of the probe pulse depends linearly on the change in the quantum occupation number induced by the pump pulse. In the time scale of 50 ps, the reflectance traces indicate three distinct dynamical processes in the material: (i) drop of the reflectivity signal within 200 fs, (ii) its subsequent rise within 1 ps, and (iii) much longer process of tens picoseconds. First two processes are associated with collective excitations and photoexcitation of QPs in $FeSe_{0.8}Te_{0.2}$. A gradual increase in the excitation energy results in a proportional increase in QPs density. Moreover, the QPs decay rate slows down as the excitation fluence increases. As a consequence, transient measurements manifest a gradual time-shift of the minimum on the reflectivity diagram (Fig. 1a). The characteristic time of the process (ii) shows a linear increase with excitation fluence (inset of Fig. 1a), while the process (i) is more complex. Process (ii) reflects the *e*-phonon interaction, which is the dominant mechanism in QPs dynamics at the given time frame. Process (iii) is associated with phonon–phonon scattering demonstrating a decrease of its characteristic time as excitation increases. It should be noted that process (iii) starts after a few picoseconds and is associated with strong phonon–phonon scattering that may contribute to additional lattice distortion of the material. As a consequence, this distortion alters the electronic density of states. At this stage, the system is still in a highly excited nonequilibrium state, which consecutively alters the relative change of the reflectivity coefficient to positive values.

The photoinduced QP relaxation time is determined by the electron–phonon coupling strength in metals [14]:

$$T_e = \frac{3\hbar\lambda < \omega^2 >}{\pi k_B}\tau_{e-ph}, \quad (1)$$

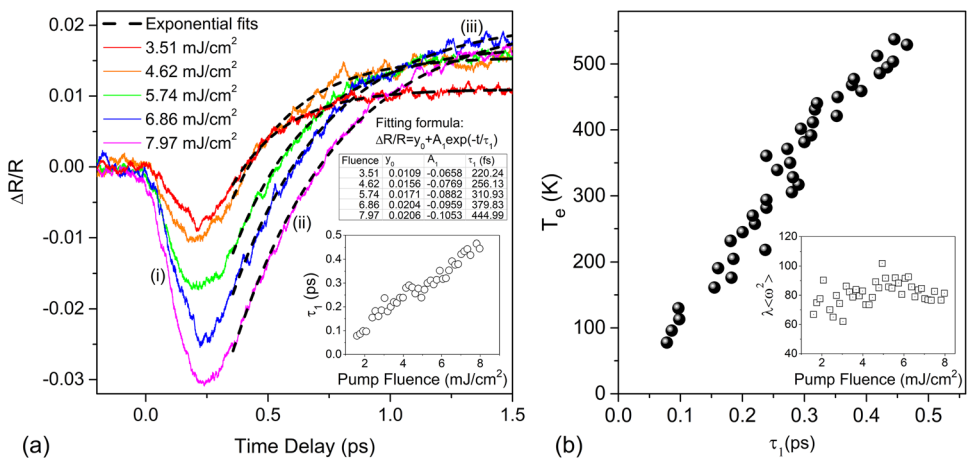

Fig. 1 **a** Power-dependent transient reflectivity at 8 K with fitting curves. The inset shows the relaxation time τ_1 vs pump fluence, as obtained from exponential fitting. The fitting formula and parameters for the traces are mentioned. **b** Adjusted temperature of electronic subsystem vs relaxation times τ_1. The inset shows obtained values for the second moment of Eliashberg function

where $\lambda < \omega^2 >$ is the second moment of the Eliashberg function, $\tau_{e\text{-}ph}$ is considered to be τ_1 from exponential fits of experimental data and $T_e = T_e^{th} - T_0$, where T_e^{th} is obtained using [2, 4, 15]:

$$T_e^{th} = \left\langle \sqrt{T_l^2 + \frac{2(1-R)F}{l_S \gamma} e^{-\frac{z}{l_S}}} \right\rangle, \quad (2)$$

where R is the unperturbed reflectivity, F is the pump fluence, l_s is optical penetration depth and γ is the linear coefficient of heat capacity due to the electronic subsystem [2]. Parameters for calculation were taken from [2]. T_e^{th} was found to be in the range from 370 to 840 K. After plotting T_e^{th} vs τ_1, linear relationship of the data was observed, but with initial systematic error. That is why the value of electronic subsystem temperature was corrected by $T_0 = 290$ K. This difference in temperatures is caused by possible inaccuracies in the estimation of the optical penetration depth and the heat capacity. The adjusted temperature of the electronic subsystem T_e vs τ_1 is presented in Fig. 1b.

Using Eq. (1) the second moment of the Eliashberg function was found to be $\lambda < \omega^2 >= 81 \pm 15$ meV^2, the values are presented in the inset of Fig. 1b. The value is within the range of 60–100 meV^2, which is consistent with most peers [2, 4, 9]. The symmetric A_{1g} mode is coherently excited by photoexcitation and coupled efficiently at $BaFe_2As_2$ [3]. For FeSe, A_{1g} is the strongest phonon mode in electron–phonon spectral function [16]. Taking $A_{1g} = 19.9$ meV^2 as in [2], leads to $\lambda = 0.2 \pm 0.04$ meV^2, which is close to 0.16 meV^2 for FeSe [2] and its theoretical value of 0.17 meV^2 [16]. It is slightly higher than 0.11 meV^2 and 0.13 meV^2, reported for $FeSe_{0.2}Te_{0.8}$ [4], and lower than the theoretical value of 0.3 meV^2 for $FeTe_{0.5}Se_{0.5}$, reported in [17]. As for the critical temperature, for FeSe $T_c = 8.8$ K [2], we observe $T_c \sim 12$ K from resistivity temperature dependence measurements, presented in Fig. 2(c), for $FeSe_{0.8}Te_{0.2}$, close to $T_c = 10$–13.5 K for $FeSe_{0.2}Te_{0.8}$ [4], and 14.5 K for $FeSe_{0.5}Te_{0.5}$ [18]. A higher T_c of 17 K in $FeSe_{0.5}Te_{0.5}$ is measured in [19] and up to 24 K in the family of $FeSe_{1-x}Te_x$ [5–8].

Nematicity

The ultrafast optical spectroscopy presents an important tool for studying transient nematicity along with other nonequilibrium processes and phase transitions [11, 20–22]. In contrast to static, time-averaged measurements, ultrafast spectroscopy may be able to reveal temporal fluctuations in the nematic order parameter. Through femtosecond-resolved optical reflectivity $\Delta R/R$, we demonstrate a different way of obtaining key information about electronic nematicity. We detect light-induced change of the circularly-polarized probe pulse reflectance by measuring two orthogonally polarized contributions: $\Delta R_{\parallel}/R_{\parallel}(0)$ and $\Delta R_{\perp}/R_{\perp}(0)$. The differential nematicity signal defined as $\eta = \Delta R_{\parallel}/R_{\parallel}(0) - \Delta R_{\perp}/R_{\perp}(0)$ was measured at the fluence of 5.4 mJ/cm^2 (Fig. 2a, b) as a function of both temperature and time delay. As compared with optical reflection, the light-induced polarization anisotropy changes are approximately ten times smaller. However, a good signal resolution for differential reflectivity measurements makes it possible to detect key signals originating from the nematic state. During the first 200 fs upon 35-fs laser excitation, QPs are generated as an accumulation process.

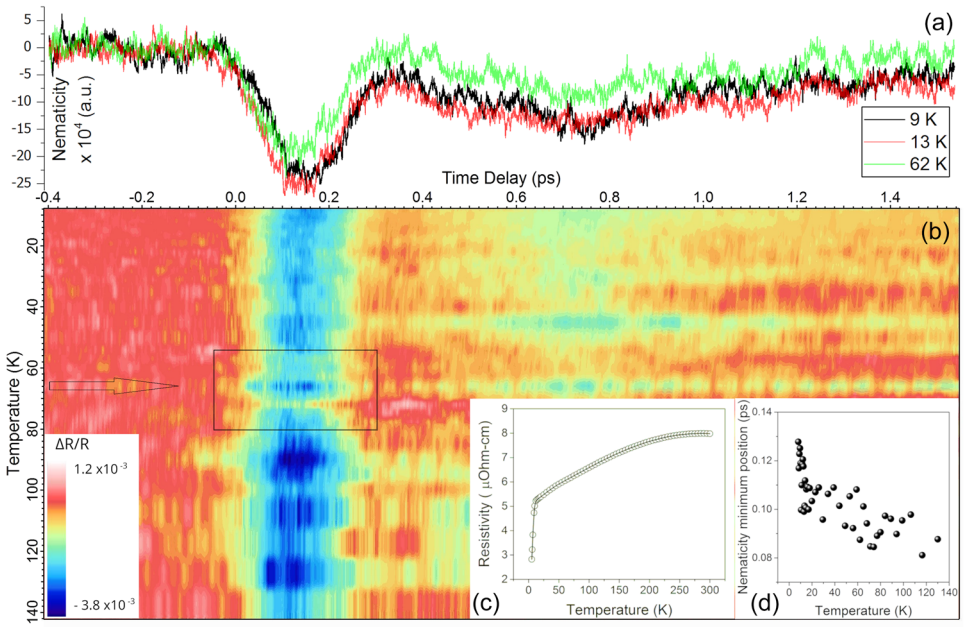

Fig. 2 **a** Nematicity signal at 9 K, 13 K and 62 K. **b** Two-dimensional map of the nematicity signal as a function of both temperature and time delay. **c** Resistivity of the superconducting film vs temperature. **d** Time delay of nematicity minimum vs temperature

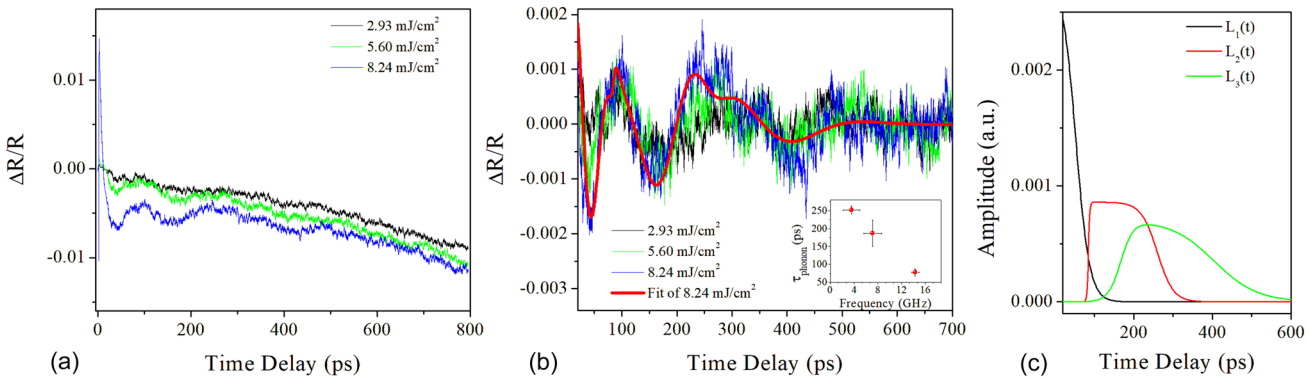

Fig. 3 **a** Transient reflectivity signal within 800 ps time scale and **b** the oscillatory part of reflectivity signal caused by coherent acoustic phonons, and a modeled signal. The inset shows the lifetimes of three phonon modes used in the model. **c** Modified logistic functions from the model

The temporal width of this response is larger than the pulse duration. The accumulation process has anisotropic character, and this results in the formation of nematicity minimum as seen in Fig. 2a. As the temperature rises, we observe very noticeable shift of nematicity minimum position that proceeds up to $T_c \sim 12$ K (Fig. 2d).

At this point, it should be noted that the delay time at the position of minima is equivalent to the characteristic time of the (i) process. This can be derived by considering two exponential functions with slightly different time constants for reflectivity signals with orthogonal polarizations measured in two different channels: $\Delta R_{\parallel}/R_{\parallel}(0) = A_0 + A_1 exp\left(-t/\tau_0\right)$ and $\Delta R_{\perp}/R_{\perp}(0) = A_0 + A_1 exp\left(-t/(\tau_0 + \Delta)\right)$. The condition $d\eta/dt = 0$ gives the time $t = \tau_0$ for the position of minima in Fig. 2a, b. In our measurements, τ_0 reduces from 130 fs to approximately 100 fs as the temperature rises from 8 to 15 K. We note that this characteristic time is difficult to evaluate directly from exponential fitting with acceptable accuracy, owing to very large fitting error.

The signature of the nematic phase transition is manifested in the increment of the nematic susceptibility when approaching structural transition. The high-temperature tetragonal symmetry of the sample is lowered to orthorhombic at the T_S temperature that, in most of the iron pnictides, is about 1–2 K higher than the nematic phase transition temperature T_N. We identify T_N to be 66 K, as indicated by the arrow in Fig. 2. The nematicity transition is manifested in a rapid change of the nematicity minimum amplitude a few degrees both below and above T_N. During the set of measurements on $FeSe_{0.8}Te_{0.2}$ samples of different thickness we detect nematic phase transition temperatures in the range from 56 to 69 K. This finding coincides with the result reported in [23].

Acoustic phonons generation

Power-dependent transient reflectivity measurements demonstrate strong acoustic phonons generation on longer time-scales, up to 1 ns. A generation of coherent acoustic phonons is the subsequent process of the stage (iii) that could provide important information about low-energy phonon interactions with QPs and/or about the final thermalization stage of the system. The signal in Fig. 3a consists of two terms: one is an exponential term due to the heat redistribution in the sample, and another one is an oscillatory term related to coherent acoustic phonons [24]. Figure 3b demonstrates the oscillatory term of the transient reflectivity data after subtraction of the exponential term. The formula used for modeling phonons is:

$$\frac{\Delta R}{R}(t) = L_1(t)\sin\left(\omega_1 t + \varphi_{01}\right) + L_2(t)\sin\left(\omega_2 t + \varphi_{02}\right) + L_3(t)\sin\left(\omega_3 t + \varphi_{03}\right), \quad (3)$$

where $\omega_3 = 2\omega_2 = 4\omega_1$, $L_i(t)$ is modified logistic function responsible for generation, duration, and decaying rate of each of the following phonon modes. From their time-dependent behavior (see Fig. 3c), it can be stated that higher frequency phonons decay into lower frequency ones. The lifetime of phonon modes τ_{phonon} was identified from the $L_i(t)$, and their dependence on the mode frequency is presented in the inset of Fig. 3b. Thomsen et al. [24] showed that the oscillations in transient reflectivity for thin films within the picosecond domain are related to the photogeneration of acoustic phonons and elastic properties of the material. In the present experiment, the acoustic phonon decay through anharmonic interaction in $FeSe_{0.8}Te_{0.2}$ and can be considered as its diffusive propagation in the film. As shown in [25], the characteristic phonon lifetime strongly depends on phonon frequency as $\tau_{phonon} \sim \omega^{-5}$. This theoretical work fully supports our current observation.

Conclusions

In summary, we have investigated power- and temperature-dependent nonequilibrium ultrafast dynamics of $FeSe_{0.8}Te_{0.2}$ by pump-probe femtosecond spectroscopy. Three distinct processes were identified and quantitatively described. Nematicity measurements were used to explore processes upon laser excitation and show strong temperature dependence in the superconducting phase. The electron–phonon relaxation times were extracted from power-dependent transient reflectance measurements, and are in the range from 100 to 500 fs in the pump fluence range from 1.6 to 8 mJ/cm^2. The temperature of the electronic subsystem was estimated, and together with electron–phonon relaxation time τ_1 was used to obtain the electron–phonon coupling constant of $\lambda = 0.2$. Three coherent acoustic phonon modes were observed, and their lifetimes were estimated.

Acknowledgments The work was supported at UPRM by the NSF Award# DMR-1905691.

Data availability The datasets generated during and/or analyzed during the current study are available from the corresponding author on reasonable request.

Declarations

Conflict of interest The authors state that they have no conflicts of interest.

References

1. C.W. Luo, P. Chung Cheng, S.H. Wang, J.C. Chiang, J.Y. Lin, K.H. Wu, J.Y. Juang, D.A. Chareev, O.S. Volkova, A.N. Vasiliev, Unveiling the hidden nematicity and spin subsystem in FeSe. npj Quantum Mater. **2**, 32 (2017). https://doi.org/10.1038/s41535-017-0036-5
2. C.W. Luo, I.H. Wu, P.C. Cheng, J.Y. Lin, K.H. Wu, T.M. Uen, J.Y. Juang, T. Kobayashi, D.A. Chareev, O.S. Volkova, A.N. Vasiliev, Quasiparticle dynamics and phonon softening in FeSe superconductors. Phys. Rev. Lett. **108**, 257006 (2012). https://doi.org/10.1103/PhysRevLett.108.257006
3. B. Mansart, D. Boschetto, A. Savoia, F. Rullier-Albenque, A. Forget, D. Colson, A. Rousse, M. Marsi, Observation of a coherent optical phonon in the iron pnictide superconductor $Ba(Fe_{1-x}Co_x)_2As_2$ (x=0.06 and 0.08). Phys. Rev. B **80**, 172504 (2009). https://doi.org/10.1103/PhysRevB.80.172504
4. Q. Wu, H. Zhou, Y. Wu, L. Hu, S. Ni, Y. Tian, F. Sun, F. Zhou, X. Dong, Z. Zhao, J. Zhao, Ultrafast quasiparticle dynamics and electron-phonon coupling in $(Li_{0.84}Fe_{0.16})OHFe_{0.98}Se$. Chinese Phys. Lett. **37**, 097802 (2020). https://doi.org/10.1088/0256-307X/37/9/097802
5. Y. Pusheng, X. Zhongtang, Y. Ma, Y. Sun, T. Tsuyoshi, Angular-dependent vortex pinning mechanism and magneto-optical characterizations of $FeSe_{0.5}Te_{0.5}$ thin films grown on CaF_2 substrates. Supercond. Sci. Technol. **29**, 035013 (2016). https://doi.org/10.1088/0953-2048/29/3/035013
6. E. Bellingeri, I. Pallecchi, R. Buzio, A. Gerbi, D. Marrè, M.R. Cimberle, M. Tropeano, M. Putti, A. Palenzona, C. Ferdeghini, $T_c = 21$ K in epitaxial $FeSe_{0.5}Te_{0.5}$ thin films with biaxial compressive strain. Appl. Phys. Lett. **96**, 102512 (2010). https://doi.org/10.1063/1.3358148
7. V. Braccini, S. Kawale, E. Reich, E. Bellingeri, L. Pellegrino, A. Sala, M. Putti, K. Higashikawa, T. Kiss, B. Holzapfel, C. Ferdeghini, Highly effective and isotropic pinning in epitaxial Fe(Se, Te) thin films grown on CaF_2 substrates. Appl. Phys. Lett. **103**, 172601 (2013). https://doi.org/10.1063/1.4826677
8. F. Fan, X. Zhongtang, Z. Cheng, H. Huang, Y. Zhu, S. Liu, C. Dong, X. Zhang, Y. Ma, Enhanced superconducting properties of $FeSe_{0.8}Te_{0.2}$ thin films grown by pulsed laser deposition. Physica C **564**, 55 (2019). https://doi.org/10.1016/j.physc.2019.06.003
9. L. Rettig, R. Cortés, H.S. Jeevan, P. Gegenwart, T. Wolf, J. Fink, U. Bovensiepen, Electron-phonon coupling in 122 Fe pnictides analyzed by femtosecond time-resolved photoemission. New J. Phys. **15**, 083023 (2013). https://doi.org/10.1088/1367-2630/15/8/083023
10. J. Orenstein, Ultrafast spectroscopy of quantum materials. Phys. Today **65**, 44–50 (2012). https://doi.org/10.1063/PT.3.1717
11. D.H. Torchinsky, G.F. Chen, J.L. Luo, N.L. Wang, N. Gedik, Band-dependent quasiparticle dynamics in single crystals of the $Ba_{0.6}K_{0.4}Fe_2As_2$ superconductor revealed by pump-probe spectroscopy. Phys. Rev. Lett. **105**, 027005 (2010). https://doi.org/10.1103/PhysRevLett.105.027005
12. J. Zhao, A.V. Bragas, R. Merlin, D.J. Lockwood, Magnon squeezing in antiferromagnetic MnF_2 and FeF_2. Phys. Rev. B **73**, 184434 (2006). https://doi.org/10.1103/PhysRevB.73.184434
13. V.V. Kabanov, J. Demsar, B. Podobnik, D. Mihailovic, Quasiparticle relaxation dynamics in superconductors with different gap structures: theory and experiments on $YBa_2Cu_3O_{7-\delta}$. Phys. Rev. B **59**, 1497–1506 (1999). https://doi.org/10.1103/PhysRevB.59.1497
14. P.B. Allen, Theory of thermal relaxation of electrons in metals. Phys. Rev. Lett. **59**, 1460–1463 (1987). https://doi.org/10.1103/PhysRevLett.59.1460
15. D. Boschetto, E.G. Gamaly, A.V. Rode, B. Luther-Davies, D. Glijer, T. Garl, O. Albert, A. Rousse, J. Etchepare, Small atomic displacements recorded in bismuth by the optical reflectivity of femtosecond laser-pulse excitations. Phys. Rev. Lett. **100**(2), 027404 (2008). https://doi.org/10.1103/PhysRevLett.100.027404
16. A. Subedi, L. Zhang, D.J. Singh, M.H. Du, Density functional study of FeS, FeSe, and FeTe: electronic structure, magnetism, phonons, and superconductivity. Phys. Rev. B **78**, 134514 (2008). https://doi.org/10.1103/PhysRevB.78.134514
17. J. Li, G. Huang, Spin-phonon coupling in the superconductor $FeTe_{0.5}Se_{0.5}$ from first-principles calculations. Solid State Commun. **159**, 45–48 (2013)
18. N. Katayama, S.D. Ji, D. Louca, S. Lee, M. Fujita, T.J. Sato, J.S. Wen, Z.J. Xu, G.D. Gu, G.Y. Xu, Z.W. Lin, M. Enoki, S. Chang, K. Yamada, J.M. Tranquada, Investigation of the spin-glass regime between the antiferromagnetic and superconducting phases in $Fe_{1+y}Se_xTe_{1-x}$. J. Phys. Soc. Jpn. **79**, 113702 (2010). https://doi.org/10.1143/JPSJ.79.113702
19. W. Si, Z.W. Lin, Q. Jie, W.G. Yin, J. Zhou, G. Genda, P.D. Johnson, Q. Li, Enhanced superconducting transition temperature in $FeSe_{0.5}Te_{0.5}$ thin films. Appl. Phys. Lett. **95**, 052504 (2009). https://doi.org/10.1063/1.3195076
20. L. Rettig, R. Cortés, S. Thirupathaiah, P. Gegenwart, H.S. Jeevan, M. Wolf, J. Fink, U. Bovensiepen, Ultrafast momentum-dependent response of electrons in antiferromagnetic $EuFe_2As_2$ driven by optical excitation. Phys. Rev. Lett. **108**, 097002 (2012). https://doi.org/10.1103/PhysRevLett.108.097002

21. T. Li, A. Patz, L. Mouchliadis, J. Yan, T.A. Lograsso, I.E. Perakis, J. Wang, Femtosecond switching of magnetism via strongly correlated spin–charge quantum excitations. Nature **496**, 69–73 (2013). https://doi.org/10.1038/nature11934
22. K.W. Kim, A. Pashkin, H. Schäfer, M. Beyer, M. Porer, T. Wolf, C. Bernhard, J. Demsar, R. Huber, A. Leitenstorfer, Ultrafast transient generation of spin-density-wave order in the normal state of $BaFe_2As_2$ driven by coherent lattice vibrations. Nat. Mater. **11**, 497–501 (2012). https://doi.org/10.1038/nmat3294
23. K. Mukasa, K. Matsuura, M. Qiu, M. Saito, Y. Sugimura, K. Ishida, M. Otani, Y. Onishi, Y. Mizukami, K. Hashimoto, J. Gouchi, R. Kumai, Y. Uwatoko, T. Shibauchi, High-pressure phase diagrams of $FeSe_{1-x}Te_x$: correlation between suppressed nematicity and enhanced superconductivity. Nat. Commun. **12**, 381 (2021). https://doi.org/10.1038/s41467-020-20621-2
24. C. Thomsen, J. Strait, Z. Vardeny, H.J. Maris, J. Tauc, J.J. Hauser, Coherent phonon generation and detection by picosecond light pulses. Phys. Rev. Lett. **53**, 989 (1984). https://doi.org/10.1103/PhysRevLett.53.989
25. R. Orbach, L.A. Vredevoe, The attenuation of high frequency phonons at low temperatures. Physics **1**, 914 (1964). https://doi.org/10.1103/PhysicsPhysiqueFizika.1.91